

Vibration isolation for scanning tunneling microscopy

M. Okano, K. Kajimura, S. Wakiyama, F. Sakai, W. Mizutani, and M. Ono

Citation: *Journal of Vacuum Science & Technology A* **5**, 3313 (1987); doi: 10.1116/1.574189

View online: <http://dx.doi.org/10.1116/1.574189>

View Table of Contents: <http://scitation.aip.org/content/avs/journal/jvsta/5/6?ver=pdfcov>

Published by the AVS: Science & Technology of Materials, Interfaces, and Processing

Articles you may be interested in

[Systematic analyses of vibration noise of a vibration isolation system for high-resolution scanning tunneling microscopes](#)

Rev. Sci. Instrum. **82**, 083702 (2011); 10.1063/1.3622507

[Vibration compensation for high speed scanning tunneling microscopy](#)

Rev. Sci. Instrum. **70**, 4600 (1999); 10.1063/1.1150119

[Theory of scanning tunneling microscopy](#)


J. Vac. Sci. Technol. B **12**, 2189 (1994); 10.1116/1.587738

[Vibration isolation analysis for a scanning tunneling microscope](#)





Rev. Sci. Instrum. **63**, 3326 (1992); 10.1063/1.1142547

[Theories of the feedback and vibration isolation systems for the scanning tunneling microscope](#)

Rev. Sci. Instrum. **58**, 2004 (1987); 10.1063/1.1139507



Instruments for Advanced Science

<p>Contact Hiden Analytical for further details: W www.HidenAnalytical.com E info@hiden.co.uk CLICK TO VIEW our product catalogue</p>	 <p>Gas Analysis</p> <ul style="list-style-type: none"> › dynamic measurement of reaction gas streams › catalysis and thermal analysis › molecular beam studies › dissolved species probes › fermentation, environmental and ecological studies 	 <p>Surface Science</p> <ul style="list-style-type: none"> › UHV-TPD › SIMS › end point detection in ion beam etch › elemental imaging - surface mapping 	 <p>Plasma Diagnostics</p> <ul style="list-style-type: none"> › plasma source characterization › etch and deposition process reaction › kinetic studies › analysis of neutral and radical species 	 <p>Vacuum Analysis</p> <ul style="list-style-type: none"> › partial pressure measurement and control of process gases › reactive sputter process control › vacuum diagnostics › vacuum coating process monitoring
---	--	--	--	--

Vibration isolation for scanning tunneling microscopy

M. Okano, K. Kajimura, S. Wakiyama,^{a)} F. Sakai,^{a)} W. Mizutani, and M. Ono
Electrotechnical Laboratory, Sakuramura, Ibaraki 305, Japan

(Received 7 April 1987; accepted 21 June 1987)

Vibration isolation technology for scanning tunneling microscopy (STM) to suppress the external mechanical perturbation down to a subatomic scale is described. The system is simplified into two subsystems, a tunneling assembly and a supporting table. Each of them has its own mechanical eigenfrequency. The principle of the isolation exists in making the two eigenfrequencies very different from each other. A theory of isolation developed is based on a model of multiply coupled oscillators with damping. Experimental results of the isolation characteristics for the two types of isolators constructed, one consisting of two-stage coil springs and the other of multiply stacked metal plates with rubber pieces among them, are well explained by the theory. STM images of graphite are obtained by using these isolators combined with various tunneling assemblies. Thereby the basis for design of the isolators is clarified.

I. INTRODUCTION

It has turned out that the scanning tunneling microscope (STM) is effective for the study of surface atomic structures since Binnig *et al.* revealed the 7×7 superstructure of Si(111) surface by using an STM.¹ The STM utilizes the high sensitivity of tunneling current flowing through the gap between a conducting sample and a metal tip. Operation of STM is based on mapping of the surface height distribution of the sample by scanning the fine metal tip above the sample, keeping the tunneling current constant. The tunneling current is so sensitive to the gap distance that the surface structure of the sample is obtained in an atomic scale with a tip of a single atom.

The STM consists of a tunneling assembly, an electrical control circuit, and a vibration isolator. The tunneling assembly possesses a probing metal tip, a sample to be observed, and coarse and fine positioners. The control circuit measures the tunneling current with high precision and controls the fine positioners and scanners to keep the tunneling current constant. The vibration isolator suppresses the change in the distance between the probing metal tip and the sample due to the external mechanical vibration. Technologies of surface cleaning and data processings such as digital noise reduction or three-dimensional imaging are also essential for STM.

In this paper we report the vibration isolation technology to suppress the external perturbation down to a subatomic scale, e.g., 1 pm. We shall simplify the mechanical system of an STM by dividing it into two subsystems: the tunneling assembly and a supporting table. Each of them has its own mechanical eigenfrequency. The principle of vibration isolation is to make the ratio of the two eigenfrequencies greater than at least two orders of magnitude.

Three types of vibration isolator have been reported so far for STM: magnetic levitation utilizing the superconducting Meissner effect,² two-stage coil-spring suspension,³ and multiply stacked metal plates with rubber pieces among them.³ The magnetic levitation has not been widely used since it requires liquid He and has undesirable effects, e.g., thermal isolation between the vibration isolator and the tunneling assembly is not sufficient and therefore the thermal

stress relaxing over a long time causes thermal drift of STM images. Although the latter two types, especially the metal-stack isolators, are widely used at present, only the principle of vibration isolation of them has been reported.⁴

In Sec. II we develop a general theory and a design rule of vibration isolation based on the calculation for multiply coupled oscillators having dampers. In Sec. III, we describe experimental results of the isolation performance for two types of isolators and compare them with theoretical calculations. In Sec. IV examples of observation of surface atomic images are shown for highly oriented pyrolytic graphite using these isolators combined with various tunneling assemblies. Concluding remarks are mentioned in Sec. V.

II. THEORY OF VIBRATION ISOLATION FOR STM

A. General consideration of vibration isolation

External vibrations coming along a building floor have wide varieties in their frequencies, vibration modes, and amplitudes, and all of them change with time.

Change in acceleration magnitude M at different floors of the main building of the Electrotechnical Laboratory is shown in Fig. 1 as a function of mechanical oscillation frequency f . The acceleration magnitude was measured during working hours with an acceleration sensor having a resolution of $10^{-5}g$, where g is the acceleration of gravity (9.8 m/s^2). The vibration amplitude a is given by $a = M / (2\pi f)^2$. Depending on the floors, the frequency components and vibration modes were considerably different. The acceleration magnitude at the third floor reached the maximum of $6 \times 10^{-5}g$ at 180 Hz, corresponding to the amplitude of 0.46 nm, which is far greater than an atomic scale. The level of the vibration amplitude to be achieved at the tunneling assembly is 1 pm, i.e., a few tenths of the surface atomic corrugation amplitude of metals.

If the eigenfrequency of the tunneling assembly is raised to be at least two orders of magnitude higher than the frequency at which the vibration amplitude of the building floor exceeds the atomic scale, it is not necessary to install the vibration isolator for an STM. However, it is not easy in general to make the eigenfrequency of the tunneling assem-

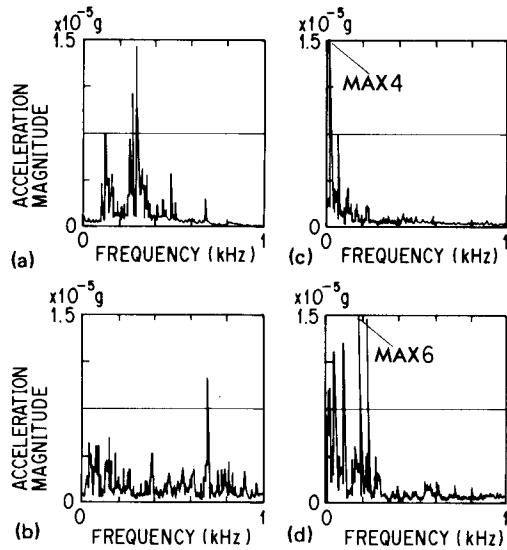


FIG. 1. Acceleration magnitude at different laboratory floors as a function of mechanical oscillation frequency: (a) Basement, (b) first floor, (c) different first floor, and (d) third floor.

bly higher than 10 kHz, since in a practical STM the tunneling assembly has to have massive parts, such as fine and coarse positioners.

B. Oscillator model of isolator and tunneling assembly

In order to simplify the principle of vibration isolation, we start by describing the isolator and the tunneling assembly with two coupled oscillators having masses m_i , m_t ($m_i \gg m_t$) and spring constants k_i , k_t without damping, as illustrated in Fig. 2. Equations of motion for the coupled oscillators are given by

$$m_i \ddot{x}_i + k_i x_i + k_t (x_i - x_t) = k_i x_b \sin \omega t, \quad (1)$$

$$m_t \ddot{x}_t + k_t (x_t - x_i) = 0, \quad (2)$$

where $x_b \sin \omega t$ is the displacement of the floor. The transfer function defined for the vibration isolator versus the floor

$$Z_i = 20 \log(x_i/x_b)$$

and that defined for the tunneling assembly versus the vibration isolator

$$Z_t = 20 \log[(x_t - x_i)/x_i]$$

are plotted as curves I and II, respectively, in Fig. 3. The abscissa denotes the oscillation frequency ω normalized by the eigenfrequency of the vibration isolator $\omega_i = (k_i/m_i)^{1/2}$. Here, the eigenfrequency of the tunneling assembly

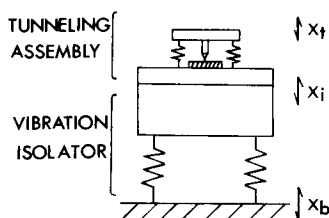


FIG. 2. Simplified model of vibration isolator and tunneling assembly.

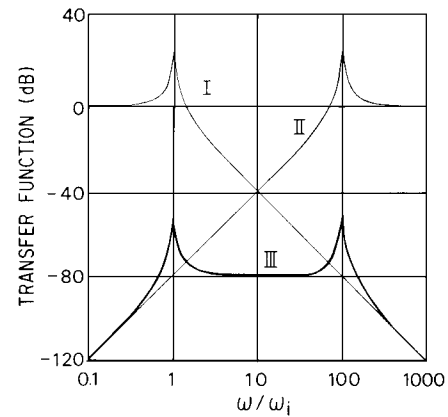


FIG. 3. Transfer function (I) defined for vibration isolator vs floor $Z_i = 20 \log(x_i/x_b)$, (II) that defined for tunneling assembly vs vibration isolator $Z_t = 20 \log[(x_t - x_i)/x_i]$, and (III) that defined for tunneling assembly vs floor. The abscissa denotes the oscillation frequency ω normalized by the eigenfrequency of the vibration isolator $\omega_i = (k_i/m_i)^{1/2}$. Here, the eigenfrequency of the tunneling assembly $\omega_t = (k_t/m_t)^{1/2}$ is chosen to be 100 times larger than ω_i .

$\omega_t = (k_t/m_t)^{1/2}$ is chosen to be 100 times larger than ω_i . The overall transfer function

$$Z = 20 \log[(x_t - x_i)/x_b]$$

is shown as curve III in Fig. 3. The peaks at two eigenfrequencies are easily reduced by adding dampings to the systems.⁴ The transfer function at the flat portion of curve III is given by $-40 \log(\omega_t/\omega_i)$ dB.

We shall see the isolation performance for a real case. In order to reduce the amplitude of $(x_t - x_i)$ at the tunneling assembly down to 1 pm, when the acceleration magnitude of $6 \times 10^{-5}g$ or the amplitude of 0.46 nm at 180 Hz shown in Fig. 1(d) comes into the system from the floor, the overall transfer function Z has to be -53 dB.

In concluding this subsection, two important items should be noted. It is necessary to evaluate the floor vibration and design the vibration isolator being suitable for individual tunneling assemblies in order to achieve the vibration amplitude of the tunneling assembly down to 1 pm. The overall isolation performance is improved by making the difference in the two eigenfrequencies larger and by making the slope of curve I above the eigenfrequency steeper. The latter can be performed by increasing the number of stages of stacked isolators as described below.

C. Design of vibration isolator

The characteristics of vibration isolators are given by the transfer function of multiply coupled oscillators having freedom n and consisting of masses M_1, M_2, \dots, M_n ; spring constants K_1, K_2, \dots, K_n ; and damping constants C_1, C_2, \dots, C_n as shown in Fig. 4. In this figure X_1, X_2, \dots, X_n are the displacements of the masses M_1, M_2, \dots, M_n , respectively, and $y = Y_0 \sin \omega t$ is the displacement due to external forces. The equations of motion for the system are described as follows:

$$\begin{aligned} M_1 \ddot{X}_1 + C_1 \dot{X}_1 + K_1 X_1 + C_2 (\dot{X}_1 - \dot{X}_2) + K_2 (X_1 - X_2) \\ = C_1 \dot{y} + K_1 y, \end{aligned} \quad (3)$$

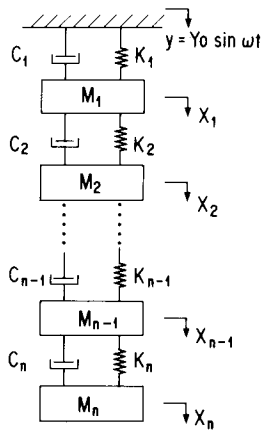


FIG. 4. Multiply coupled oscillators with freedom n consisting of masses, spring and damping constants, and modeling vibration isolators for an STM.

$$M_r \ddot{X}_r + C_r (\dot{X}_r - \dot{X}_{r-1}) + K_r (X_r - X_{r-1}) + C_{r+1} (\dot{X}_r - \dot{X}_{r+1}) + K_{r+1} (X_r - X_{r+1}) = 0 \quad (r = 2, 3, \dots, n-1), \quad (4)$$

$$M_n \ddot{X}_n + C_n (\dot{X}_n - \dot{X}_{n-1}) + K_n (X_n - X_{n-1}) = 0. \quad (5)$$

These equations are expressed by a matrix form:

$$\{[A] + j\omega[B]\}[X] = [P]. \quad (6)$$

Here, the matrix $[X]$ is the solution having a form of $X_i \exp(j\omega t)$ ($i = 1, 2, \dots, n$) and the matrices $[A]$, $[B]$, and $[P]$ are given by

$$[A] = \begin{pmatrix} K_1 + K_2 - M_1 \omega^2 & -K_2 & 0 & \dots & 0 \\ -K_2 & K_2 + K_3 - M_2 \omega^2 & -K_3 & \dots & 0 \\ 0 & \dots & \dots & \dots & \dots \\ 0 & \dots & -K_{n-1} & K_{n-1} + K_n - M_{n-1} \omega^2 & -K_n \\ 0 & \dots & \dots & -K_n & K_n - M_n \omega^2 \end{pmatrix}, \quad (7)$$

$$[B] = \begin{pmatrix} C_1 + C_2 & -C_2 & 0 & \dots & 0 \\ -C_2 & C_2 + C_3 & -C_3 & 0 & \dots \\ 0 & \dots & \dots & \dots & \dots \\ 0 & \dots & \dots & -C_n - 1 & C_{n-1} + C_n \\ 0 & \dots & \dots & 0 & -C_n \end{pmatrix}, \quad (8)$$

$$[P] = [(K_1 + j\omega C_1)Y_0, 0, \dots, 0]. \quad (9)$$

The overall transfer function Z is given by

$$Z = 20 \log(X_n/Y_0) = 20 \log\{[\operatorname{Re}(X_n)^2 + \operatorname{Im}(X_n)^2]^{1/2}/Y_0\}. \quad (10)$$

The calculated transfer function is shown in Fig. 5 for the case of freedom 2 with various damping constants. In this calculation we used the values of spring constants K_1 , K_2 and masses M_1 , M_2 of the vibration isolator with two-stage coil-spring suspension mentioned later. In the absence of damping, there exist two clear eigenfrequencies at which the vibrations are amplified infinitely. Above the upper eigenfre-

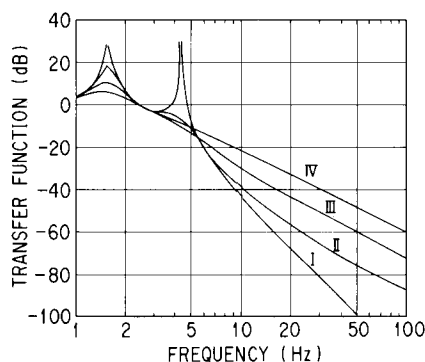


FIG. 5. Calculated transfer function for the case of freedom 2 with various damping constants. $M_1 = 2.4$ kg, $M_2 = 2.9$ kg, $k_1 = 800$ N/m, $k_2 = 700$ N/m. I: $c_1 = c_2 = 0$; II: $c_1 = c_2 = 10$ N s/m; III: $c_1 = c_2 = 20$ N s/m; IV: $c_1 = c_2 = 50$ N s/m.

quency, 4.4 Hz, the transfer function steeply decreases with frequency and results in better isolation. As the damping constant becomes larger, the peaks at the two eigenfrequencies are more suppressed. However, the transfer function above the upper eigenfrequency becomes less steep.

Figure 6 depicts the difference in the isolation performance depending on the number and placement of dampers with the same damping constant. Curve I is the case for which two dampers are placed parallel to the two springs, curve II for only one in the second stage, and curve III for only one in the first stage. The peak suppression at the eigenfrequencies is good enough for curves I and II, and the higher frequency characteristics are satisfactory for curves II and

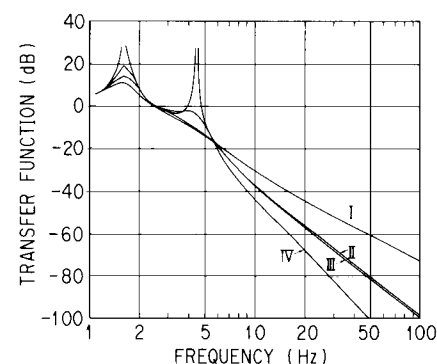


FIG. 6. Isolation performance for different placements of dampers with the same damping constant. $M_1 = 2.4$ kg, $M_2 = 2.9$ kg, $k_1 = 800$ N/m, $k_2 = 700$ N/m. I: $c_1 = c_2 = 20$ N s/m; II: $c_1 = 20$ N s/m, $c_2 = 0$; III: $c_1 = 0$, $c_2 = 20$ N s/m; IV: $c_1 = c_2 = 0$.

III. From this figure we conclude that the damper should be placed in the second stage only. The effect is verified in the experiment of the two-stage coil-suspension isolator.

Calculated transfer functions for the metal-stack isolator for various numbers of stacks are shown in Fig. 7. In this calculation we used the mass per metal plate of 1 kg and the spring constant of rubber of 6×10^4 N/m with the damping constant of 200 N s/m. Although the elastic properties of rubber are nonlinear, we used Eqs. (3)–(10) by assuming the linearity in a small-displacement approximation. The stiffness of rubber used for the metal-stack isolator is higher compared to that of coil springs, since the rubber length is limited so as not to be bent by and yield to the weight of metal plates. Therefore the eigenfrequencies are higher and the performance of the threefold isolator is poor compared to that of the spring-suspension isolator. The greater number of stacks makes the eigenfrequency lower and the isolation performance better. The metal-stack isolator can be made comparatively small in size and its isolation performance easily improved by adding conventional air-spring vibration isolators.

III. EXPERIMENTAL RESULTS OF CONSTRUCTED ISOLATORS

We have constructed two types of vibration isolators: a two-stage coil-spring suspension with eddy current dampers and metal stacks with rubber pieces among metal plates.

A. Two-stage coil-spring suspension

A schematic of the two-stage coil-spring suspension isolator is shown in Fig. 8, in which I is the base frame directly connected to a vacuum chamber or a conventional air-spring vibration isolator, II is the middle frame suspended by three coil springs from I, and III is the exterior frame suspended by three coil springs from II. Each end of the coil spring is terminated by a rubber ring in order to attenuate the high-frequency sound propagating along solid columns, frames, and coil springs. Eddy current dampers consisting of copper blocks (IV and VI in Fig. 8) and permanent magnets (V) also make the gravity center of the suspended frames lower than the horizontal plane of the three lower ends of the coil springs. The configuration prevents the translational motion along the gravity direction and the rotational motions

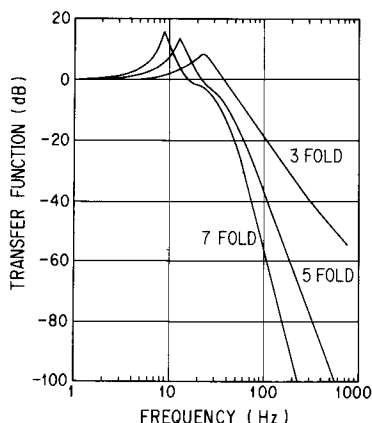


FIG. 7. Calculated transfer function of metal-stack isolator using various numbers of stacks as the parameter.

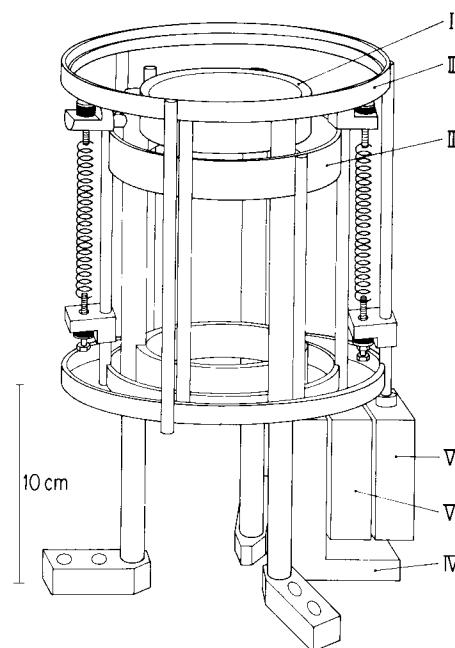


FIG. 8. Schematic of two-stage coil-spring suspension isolator. I: base frame directly connected to vacuum chamber; II: middle frame suspended by three coil springs from I; III: exterior frame suspended by three coil springs from II. Each end of the coil spring is terminated by a rubber ring. Eddy current dampers consist of copper blocks (IV and VI) and permanent magnets (V).

around the gravity center. The caging configuration of frame III on which a tunneling assembly is placed enables easy access to wiring and simplifies the exchange procedure of samples and probing metal tips.

The damping constant C for the x -directional motion of a rectangular conductor having dimensions d along the x axis, b along the y axis, and thickness t with electrical resistivity ρ , as shown in Fig. 9, placed in the magnetic induction B with a circular cross section of radius a is given by

$$C = B^2 t \pi a^2 C_0 / \rho. \quad (11)$$

The nondimensional damping constant C_0 shown in Fig. 10 was obtained for various dimensions of $2a/b$ and d/b by Nagaya,⁵ who numerically solved the Maxwell equations to satisfy boundary conditions by means of the Fourier expansion collocation method. We adopted $B = 0.2$ Wb/m², $a = 0.02$ m, $b = 0.06$ m, $d = 0.06$ m, $t = 0.02$ m, $\rho = 1.56 \times 10^{-8}$ Ω m in the two-stage spring suspension, giving $C_0 = 0.31$ and $C = 20$ N s/m.

The experimental setup in air to obtain the transfer function is shown in Fig. 11. The vibration isolator was placed on a shaker and the acceleration magnitudes at both the base

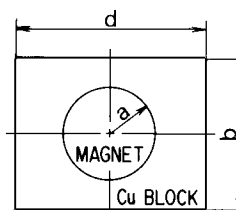


FIG. 9. Schematic of rectangular conductor having dimensions d along the x axis, b along the y axis, and thickness t with electrical resistivity ρ placed in the magnetic induction B with a circular cross section of radius a .

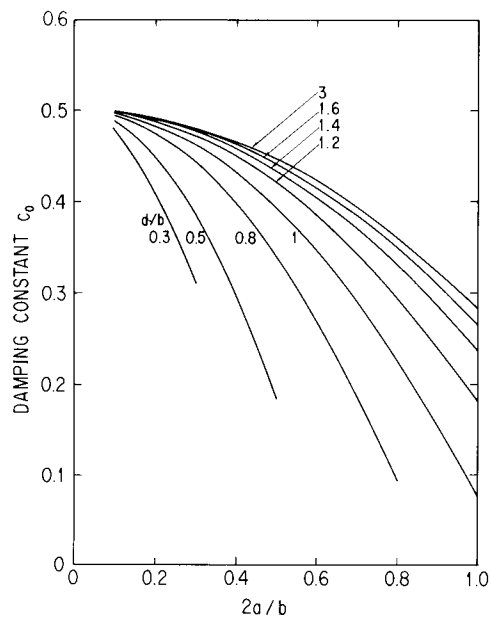


FIG. 10. Nondimensional damping constant C_0 obtained for various dimensions of $2a/b$ and d/b by Nagaya (Ref. 5).

plate and the fused quartz plate fixed on the upper frame of III in Fig. 8 were measured at the same time as a function of vibration frequency. In this experiment care was taken to prevent direct external acoustic perturbation to the frames and the acceleration sensor. The damping characteristics were obtained from the decaying oscillation waveforms after giving a light push by hand.

The isolation characteristics without and with the eddy current dampers are shown in Figs. 12(a) and 12(b), respectively, together with theoretical calculations shown by dashed lines. Two eigenfrequencies are clearly identified in Fig. 12(a). The large peak around 50 Hz was caused by acoustic noise due to commercial electric power lines. The transfer function level lower than 0 dB at frequencies between 0 and 2 Hz was due to the lack of sensitivity of the acceleration sensors at the low-frequency range. The inset of Fig. 12(a) shows the waveform of free oscillation at its eigenfrequency after a light push. The oscillation continued for about 30 min. It implies that, in the absence of the dampers, the isolation performance is very steep at the higher frequency range; however, the tunneling assembly is forced to vibrate at the isolator eigenfrequency for a long time once external perturbation has been applied to the isola-

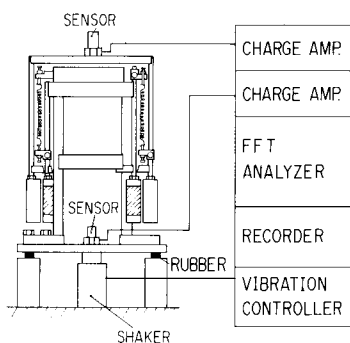


FIG. 11. Experimental setup to obtain transfer function.

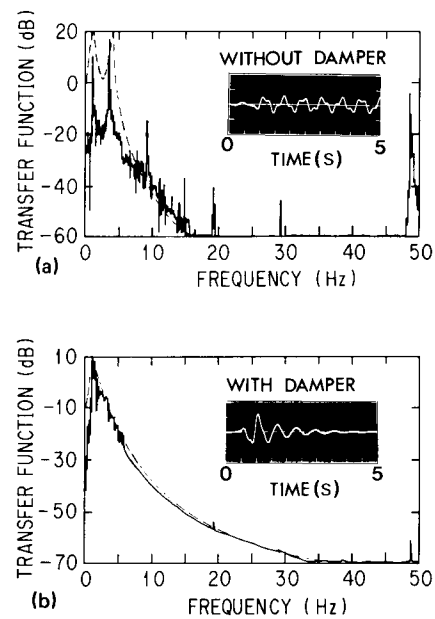


FIG. 12. (a) Transfer function of two-stage coil-spring isolator without eddy current damper and (b) with dampers. Dashed lines show theoretical calculations. Insets show waveform of free oscillation after a light push.

tor. Even if the eigenfrequency of the tunneling assembly is higher than that of the isolator, the peak at the eigenfrequency of the isolator as shown in curve III of Fig. 3 should be suppressed by dampers sufficiently to eliminate the atomic scale vibration of the tunneling assembly resulting from the external noise. In Fig. 12(b), the higher peak presented in Fig. 12(a) is suppressed by the dampers, and after a push the oscillation attenuates within a few seconds, as shown in the inset.

B. Metal-stack isolator

Figure 13 illustrates a fivefold metal-stack isolator designed such that the gravity center is located as low as possible on each metal plate. The top metal plate on which the tunneling assembly is placed is able to hold an additional weight at the lower end to adjust the position of its gravity center down to the lowest plate of the stack, depending on the weight of the tunneling assembly. The design prevents

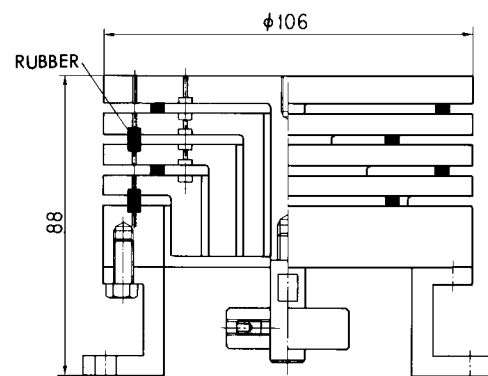


FIG. 13. Fivefold metal-stack isolator designed to locate the gravity center as low as possible for each metal plate.

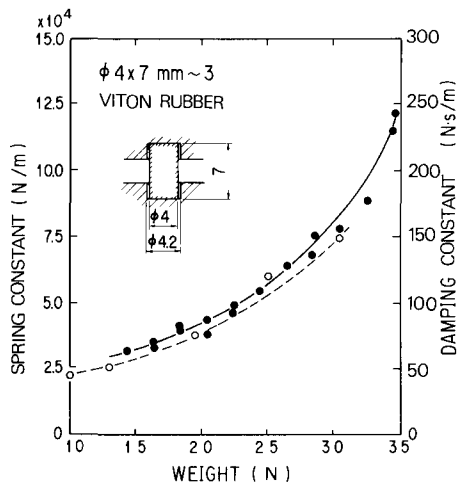


FIG. 14. Spring and damping constants of rubber as a function of weight.

oscillation coupling and gives stability against the rolling of the system. Between each metal plate three pieces of Viton rubber with 4-mm diameter and 7-mm length are placed concyclically with 90-mm diameter. The Viton rubber was chosen for use in ultrahigh vacuum. Since the spring and the damping constants of rubber are strongly dependent upon the load in this configuration, they were obtained experimentally and are shown in Fig. 14. The spring constant was obtained from the relationship between load and displacement with the twofold stack with three pieces of rubber between them. The damping constant C was determined by the relationship $C = -2M \ln(x/t)$ through the damping waveform after giving a transient displacement to the stack, where M is the mass loaded per piece of rubber and x is the displacement that occurs during the time interval t .

Figure 15 shows the transfer function and the damping waveform of the fivefold metal-stack isolator illustrated in Fig. 13. There exists only one eigenfrequency. Isolation of -60 dB at 320 Hz and a damping time as short as 0.5 s are obtained. A marked discrepancy is seen in Fig. 15 between the experimental result (solid line) and the one calculated based on the measured load dependence of spring and damping constants shown in Fig. 14 by the dashed line. The discrepancy

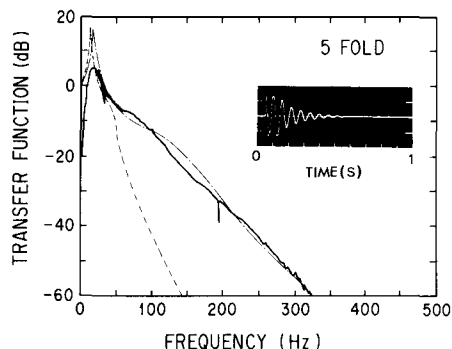


FIG. 15. Transfer function of fivefold metal-stack isolator (solid line). Dashed line is the calculated result based on the measured values of spring and damping constants shown in Fig. 14, and dash-dotted line is the calculated result based on the measured value of the spring constant of rubber as a function of frequency shown in Fig. 16. Inset shows damping waveform of free oscillation after a light push.

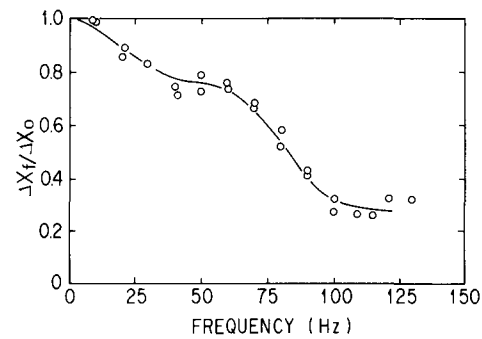


FIG. 16. Frequency dependence of the displacement Δx_f normalized by the static displacement Δx_0 of rubber.

crepancy turned out to be due to the frequency dependence of the spring and damping constants of rubber. Frequency dependence of these constants was obtained from the displacement of the twofold metal stack using an electromagnet, with which the attractive force was kept constant by controlling the coil current of the magnet against the change in driving frequency. Figure 16 shows the frequency dependence of the displacement Δx_f normalized by the static displacement Δx_0 . It is noted that the characteristic is not applicable to all kinds of rubber. The calculated result taking account of the frequency dependence is represented by the dash-dotted line in Fig. 15, explaining the experiment very well.

The isolation performance of the coil-spring isolator is better than that of the metal-stack isolator: the coil-spring isolator has -60 -dB isolation at 22 Hz, while the metal-stack isolator has the same at 320 Hz. Further improvement of the performance of the metal-stack isolator is achieved either by adding a conventional air-spring isolator, by inserting small coil springs together with or instead of rubber pieces between stacks, or by suspending the metal stack with springs.

The isolation performance of the metal stack, when rubber pieces were replaced by small springs at the lowest stack and by both rubber and springs at the second stack, is shown in Fig. 17. The spring constant of the springs used in the metal stack was 2.4×10^4 N/m. The constant should be as small as possible within the limitations of length so as not to be bent due to the load, and of stiffness so as not to be compressed.

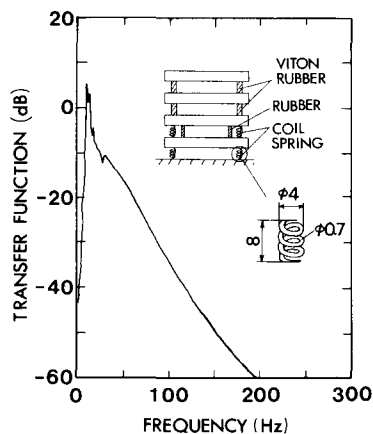


FIG. 17. Transfer function of fivefold metal stack, when rubber pieces at the lowest stack were replaced by small springs and both rubber and springs were used in the second stack.

The isolation characteristics of the metal stack, when suspended by three coil springs and three rubber strings, are shown in Figs. 18(a) and 18(b), respectively. The eigenfrequency is clearly decreased down to several Hz and the isolation performance is improved. The shaggy structures above 100 Hz in Fig. 18(a) are due to the transverse *string oscillation* of the coil spring. At around 150 Hz the string oscillation was able to be recognized even by eye and ear. Although the isolation performance of Fig. 18(b) is almost the same as that of Fig. 18(a), the high-frequency characteristics are much improved by the rubber string suspension.

To summarize this section, we compare the isolation performance of various isolators in Fig. 19: (a) two-stage coil-spring suspended isolator; (b) fivefold metal-stack isolator alone, (c) fivefold metal-stack isolator with coil-spring suspension, and (d) fivefold metal-stack isolator with rubber-string suspension. In Fig. 19(a), there exist vibrations around 300 Hz arising from the transverse string oscillation and its higher harmonics: the peak amplitude at 340 Hz reaches 0.02 nm. If the eigenfrequency of tunneling assemblies is located around this frequency the atomic scale observation may be heavily disturbed. In the other three isolators, the high-frequency structures, which mainly arise from the sound coming into the isolator through the air, are not remarkable and are able to be completely suppressed when the systems are placed in vacuum.

IV. COMBINATION WITH TUNNELING ASSEMBLY AND STM OBSERVATION

We have constructed various types of tunneling assemblies. The tunneling assembly possessing a piezoelectric transducer (PZT)-tripod tip scanner and a magnetic-kicker-type coarse positioner is shown in Fig. 20. Since the coarse positioner is simply placed on a fused-quartz plate on a permanent magnet and there is little remnant mechanical stress,

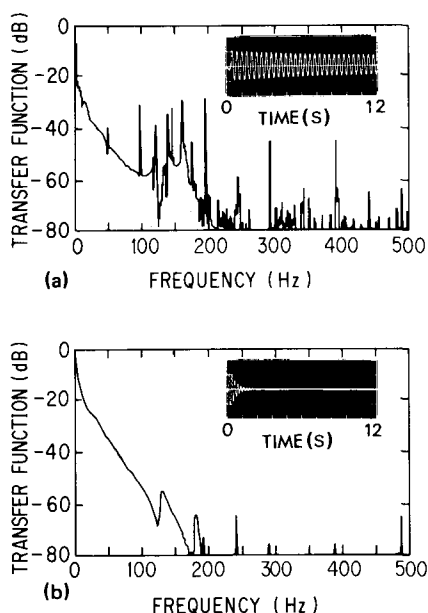


FIG. 18. (a) Transfer function of fivefold metal-stack isolator suspended by three coil springs. (b) Transfer function of metal-stack isolator suspended by three rubber strings. Inset shows damping waveform after a light push.

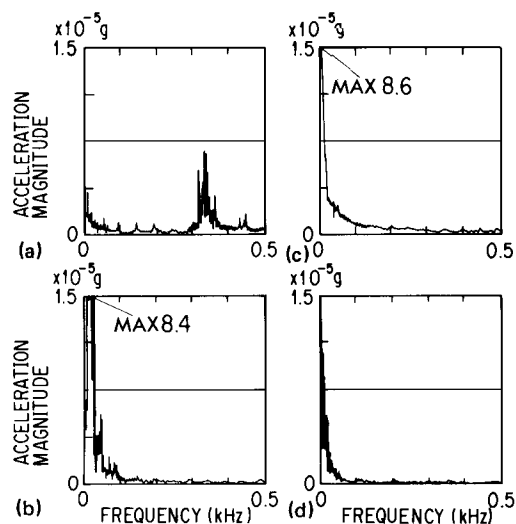


FIG. 19. Comparison of isolation performance of various isolators: (a) two-stage coil spring suspended, (b) fivefold metal stack without suspension, (c) fivefold metal stack with coil-spring suspension, and (d) fivefold metal stack with rubber-string suspension.

it moves smoothly. However, it is not stiff or rigid against external perturbation because it is constructed as a combination of many components such as a sample, a sample holder, coarse and fine positioners, and a metal probing tip. The eigenfrequency of the tunneling assembly was determined by the frequency spectrum analysis of the tunneling current to be 0.7 kHz. For this tunneling assembly with comparatively low eigenfrequency, it is necessary to employ the vibration isolator with the eigenfrequency of several Hz and with high isolation performance at the high-frequency region. The tunneling assembly held at the top of the two-stage coil-spring isolator was installed in a vacuum chamber of 10^{-8} Torr, which was placed on an air-spring isolator with the eigenfrequency of 2.2 Hz, to observe the surface atomic image of 2H-NbSe_2 at room temperature. Experimental details and discussion are described elsewhere.^{6,7}

A schematic⁸ of the metal-stack vibration isolator and a tunneling assembly utilizing a lever-type coarse positioner⁹ and a cubic PZT fine positioner¹⁰ for scanning the metal probing tip is shown in Fig. 21. The arm, on one end of which a sample is mounted, consists of two stainless-steel pieces, which are connected with plate springs. A micrometer having differential screws of $25\text{ }\mu\text{m/rotation}$ is coupled to a rotary feedthrough and actuated from outside the vacuum

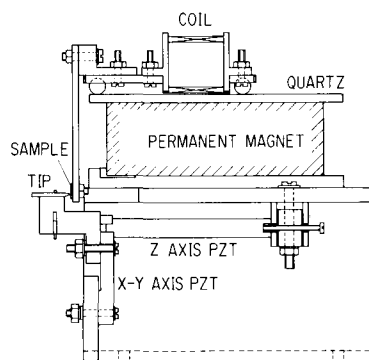


FIG. 20. Structure of the tunneling assembly possessing PZT-tripod scanner and magnetic-kicker-type coarse positioner.

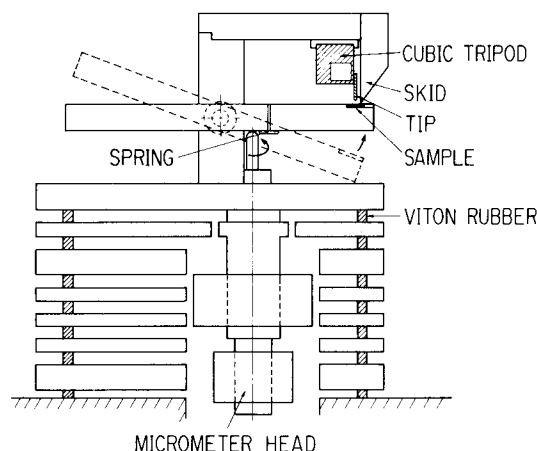


FIG. 21. Schematic of metal-stack vibration isolator and tunneling assembly utilizing lever-type coarse positioner and cubic PZT fine positioner for scanning a probing tip.

chamber. The arm pushed up with a micrometer head initially stops at the skid. The metal probing tip is mounted ~ 0.1 mm above the sample surface when the arm hits the edge of the skid. The movement of the sample is magnified, since the pivot-skid edge separation is 50 mm while the pivot-micrometer head separation is 10 mm. After the arm hits the skid, the edge of the skid acts as a new pivot to demagnify the movement of the sample since the skid edge-tip separation is less than 0.5 mm; thereby the sample-tip distance decreases very smoothly into the tunneling regime. The translational reduction of $\sim 100:1$ provides about 0.7-nm movement of the sample-probing tip distance per degree of rotation of the differential screw of the micrometer. Since the direct contact between the sample holder and the skid increased the stiffness of the tunneling assembly up to several kHz and the micrometer was actuated from outside the chamber, we were able to use the relatively rigid metal-stack isolator with higher eigenfrequency to observe the surface atomic image of highly oriented pyrolytic graphite in air as shown in Figs. 22(a) and 22(b). Experimental details will be published in the near future.¹¹

V. CONCLUSIONS

The technology of vibration isolation which suppresses the external perturbation down to a subatomic scale, e.g., 1 pm, has been described. We simplified the mechanical system with two subsystems: the tunneling assembly and the supporting table; each of them had its own mechanical eigenfrequencies. The principle of vibration isolation existed here in making the two eigenfrequencies very different from each other.

We developed a general theory of vibration isolation based on the calculation for multiply coupled oscillators with damping. Construction of two types of isolators for STM, two-stage coil-spring suspension and multiply stacked metal plates with rubber pieces among them, were described in Sec.

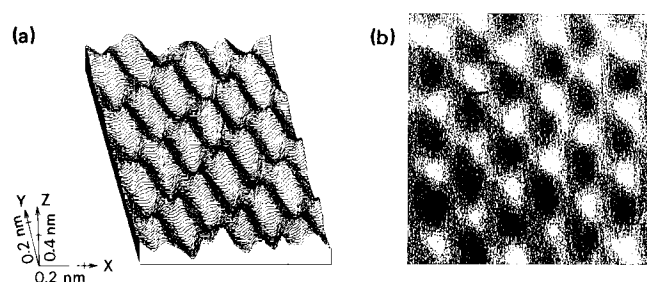


FIG. 22. Surface atomic image of highly oriented pyrolytic graphite obtained in the air: (a) three-dimensional view and (b) gray scale map. A picture frame consists of 128 rasters each containing 256 data points. The scale is 0.8×0.8 nm.

III. Experimental results of the isolation performance for the two types of isolators were well explained by the theoretical calculations based on the model, when the weight and frequency dependencies of the spring and damping constants of rubber were taken into account; thereby the design rule of vibration isolators was established. Although the metal-stack isolator had less effective performance than that of the coil-spring suspension isolators, the former was able to be made small in size, easy to handle, and it could be improved by combination with coils or rubber strings.

Surface atomic images of highly oriented pyrolytic graphite were shown as an example of successful application of these vibration isolators combined with various tunneling assemblies.

ACKNOWLEDGMENTS

The authors are grateful for discussions with H. Bando, H. Murakami, S. Okayama, H. Tokumoto, and K. Watanabe in performing the STM experiments.

^{a1} Permanent address: Seiko Instruments and Electronics, Ltd., 563 Takatsukashinden, Matsudo, Chiba 271, Japan.

¹G. Binnig, H. Rohrer, Ch. Gerber, and E. Weibel, *Phys. Rev. Lett.* **49**, 57 (1982); **50**, 120 (1982).

²G. Binnig, H. Rohrer, Ch. Gerber, and E. Weibel, *Appl. Phys. Lett.* **40**, 178 (1982).

³G. Binnig and H. Rohrer, *IBM J. Res. Dev.* **30**, 355 (1986).

⁴D. W. Pohl, *IBM J. Res. Dev.* **30**, 417 (1986).

⁵K. Nagaya, *J. Dynam. Syst. Meas. Control.* **106**, 52 (1984).

⁶H. Tokumoto, H. Bando, W. Mizutani, M. Okano, M. Ono, H. Murakami, S. Okayama, Y. Ono, K. Watanabe, S. Wakiyama, F. Sakai, K. Endo, and K. Kajimura, *Jpn. J. Appl. Phys.* **25**, L621 (1986).

⁷H. Bando, H. Tokumoto, W. Mizutani, K. Watanabe, M. Okano, M. Ono, H. Murakami, S. Okayama, Y. Ono, S. Wakiyama, F. Sakai, K. Endo, and K. Kajimura, *Jpn. J. Appl. Phys.* **26**, L41 (1987).

⁸M. Ono, S. Okayama, F. Sakai, S. Wakiyama, K. Watanabe, H. Bando, H. Murakami, H. Tokumoto, and K. Kajimura (unpublished).

⁹J. E. Demuth, R. J. Hamers, R. M. Tromp, and M. E. Welland, *IBM J. Res. Dev.* **30**, 396 (1986).

¹⁰S. Okayama, H. Bando, H. Tokumoto, and K. Kajimura, *Jpn. J. Appl. Phys.* **24**, Suppl. 24-3, 152 (1985).

¹¹H. Tokumoto, S. Okayama, S. Wakiyama, M. Shigeno, W. Mizutani, K. Sugihara, H. Bando, H. Murakami, M. Ono, and K. Kajimura (unpublished).